EUROPEAN ORGANIZATION FOR NUCLEAR RESEARCH

CERN–PPE/92-141
30 July 1992

RIKEN-AF-NP-129

ATOMIC BEAM MAGNETIC RESONANCE APPARATUS FOR SYSTEMATIC MEASUREMENT OF HYPERFINE STRUCTURE ANOMALIES (BOHR-WEISSKOPF EFFECT)

H.T. Duong[1)], C. Ekström[2)], M. Gustafsson [3)], T.T. Inamura[4)], P. Juncar[5)], P. Lievens[6)], I. Lindgren[3)], S. Matsuki[7)], T. Murayama[8)], R. Neugart [9)], T. Nilsson[3)], T. Nomura[10)], M. Pellarin[11)], S. Penselin[12)], J. Persson[3)], J. Pinard[1)], I. Ragnarsson[13)], O. Redi[14)], H.H. Stroke [14,15)], J.L. Vialle[11)] and the ISOLDE Collaboration, PPE Div., CERN, Geneva, Switzerland

Abstract

An atomic beam magnetic resonance (ABMR) apparatus has been constructed at Orsay, and has been installed at the CERN PS Booster ISOLDE mass separator facility for "on-line" work with radioactive isotopes in a program to measure hyperfine structure anomalies (the Bohr-Weisskopf effect) over long isotopic chains. The hfs anomalies result from the effect of the spatial distribution of the nuclear magnetization on the atomic hfs interaction. Constructional details of the system are described: emphasis is placed on the measurement of nuclear g-factors by a triple resonance, laser state selected, ABMR method. A precision better than 10^{-4} for g_I values has been obtained in stable atomic beam tests, leading to hfs anomaly measurements better than 10 percent. Two types of detection systems are described - laser fluorescence and surface ionization coupled with mass spectrometry.

(IS 306)

Submitted to Nuclear Instruments and Methods A

1) Laboratoire Aimé Cotton, CNRS II, Bât. 505, Faculté des Sciences, F-91405 Orsay Cedex, France
2) The Svedberg Laboratory, Uppsala University, P.O.B. 533, S-75121 Uppsala, Sweden
3) Department of Physics, Chalmers University of Technology, S-41296 Göteborg, Sweden
4) Cyclotron Laboratory, RIKEN (The Institute of Physical and Chemical Research), Hirosawa 2-1, Wako-shi, Saitama, 351-01 Japan
5) Institut National de Métrologie du CNAM, 292 rue St. Martin, F-75141 Paris Cedex 03, France (unité associée au CNRS: URA 827)
6) CERN, CH1211 Geneva 23, Switzerland
7) Nuclear Science Division, Institute of Chemical Research, Kyoto University, Gokasho, Uji-shi, Kyoto, 611 Japan
8) Tokyo University of Mercantile Marine, 2-1-6 Etchujima, Koto-ku, Tokyo, 135 Japan; on leave 1991-92 at Laboratoire Aimé Cotton, Orsay
9) Institut für Physik, Universität Mainz, Staudinger Weg 7, D-6500 Mainz, Germany
10) Institute for Nuclear Study, Tokyo University, Tanashi-shi, Tokyo, 188 Japan
11) Laboratoire de Spectrométrie Ionique et Moléculaire, Université de Lyon I, F-69622 Villeurbanne Cedex, France
12) Institut für Angewandte Physik, Universität Bonn, Wegelerstrasse 8, D-5300 Bonn 1, Germany
13) Department of Mathematical Physics, Lund Institute of Technology, P.O.B. 118, S-22100 Lund, Sweden
14) Department of Physics, New York University, New York, NY 10003, USA
15) On leave 1991-92 as Scientific Associate at CERN, Geneva, and Professeur Invité at the Faculté des Sciences, Université de Paris 11, Orsay

1 Introduction

Isotope shifts (IS) in optical atomic transitions have been measured for many years on long chains of radioactive isotopes, allowing a study of the variation of the nuclear mean square charge radius when neutrons are added to a reference nucleus. These studies have been very fruitful in the understanding of nuclear structure and have revealed a number of unexpected features.[1] In 1950, Bohr and Weisskopf[2] pointed out that, similarly, an extended nuclear magnetization has observable consequences on atomic spectra as it modifies the form of the hyperfine structure (hfs) interaction. Physically, the optical electron creates a non-uniform magnetic field over the region of the nucleus, and the interaction therefore depends on the distribution of nuclear magnetization. This leads to an "anomaly" in the hfs interaction, the *Bohr- Weisskopf (BW) effect*, the interaction being slightly different from the value that it would have for a hypothetical point nucleus. Inversely, a measurement of the Bohr-Weisskopf correction ε_{BW} to the point nuclear interaction can provide information on the distribution of spin and orbital moments in the nuclear volume, and can thus serve as a new, independent, test for nuclear models.

We note at the outset that, as in the case of isotope shifts, only ${}^1\Delta^2$, the Bohr-Weisskopf effect of isotope 1 relative to isotope 2, is measured. A direct determination of ε_{BW} would require a precision in the calculation of the point nuclear interaction much better than ~ 1 percent which is currently obtained. [3] Furthermore, for the differential Bohr-Weisskopf effect, ${}^1\Delta^2$, the *Breit-Rosenthal correction*[4], ε_{BR}, which reflects the effect of the extended nuclear charge distribution on the hfs interaction, becomes negligible.

The determination of ${}^1\Delta^2$ for a long isotopic chain requires highly precise and sensitive techniques since the effect tends to be small and the measurements involve radioactive isotopes produced at very low rates. (These rates are insufficient to obtain nuclear magnetic moments by NMR, which are usually required to determine Δ). The experimental setup described is designed for a systematic measurement of the Bohr-Weisskopf effect in a sequence of radioactive cesium isotopes to be done on-line with use of the new PSB-ISOLDE (PSB, proton synchrotron booster) mass separator facility at CERN. A triple resonance ABMR apparatus, with state selection by laser optical pumping was constructed for this work and the achieved performance studied off-line with stable potassium and rubidium atoms.

2 Bohr-Weisskopf effect or hfs anomaly

2.1 Theory

For radioactive isotopes, for which the number of atoms is insufficient to perform bulk NMR experiments, nuclear magnetic moments, $\mu_I = g_I I \mu_N$ (g_I, nuclear g-factor, I, nuclear spin, μ_N, nuclear magneton) are generally evaluated from measured magnetic dipole constants *"a"* in the hfs interaction by direct comparison with known values of I_{ref}, μ_{ref} and a_{ref} in a stable isotope of the same element as a reference, for which the NMR experiment is possible:

$$\frac{\mu}{\mu_{ref}} = \frac{aI}{a_{ref} I_{ref}} \qquad or \qquad \frac{g}{g_{ref}} = \frac{a}{a_{ref}}. \tag{1}$$

The *hfs anomaly* may, however, affect significantly the results obtained from (1), at a level of precision better than ~ 1 percent. In the ground state of the heavier alkali elements, neglecting the Breit-Rosenthal effect described in sec. 1, the main contribution to the hfs anomaly arises from the distribution of nuclear magnetization over the extended

nuclear volume. The *hfs anomaly*, or so-called *Bohr-Weisskopf effect* ε (we now drop the subscript BW), is defined by

$$a = a_{pt}(1+\varepsilon), \tag{2}$$

where a is the measured magnetic dipole hfs interaction constant and a_{pt} the value corresponding to a point nucleus. For a pair of isotopes, the differential hfs anomaly $^1\Delta^2$ is defined by

$$\frac{a_1}{a_2} = \frac{a_{pt1}(1+\varepsilon_1)}{a_{pt2}(1+\varepsilon_2)} = \frac{g_1(1+\varepsilon_1)}{g_2(1+\varepsilon_2)} \qquad or \qquad \frac{a_1}{a_2} \approx \frac{g_1}{g_2}(1+{}^1\Delta^2), \tag{3}$$

where, for small values of ε, $^1\Delta^2$ is given by

$$^1\Delta^2 = \varepsilon_1 - \varepsilon_2. \tag{4}$$

Since the effect is generally of the order of less than one percent, it is seen from (3) that, in order to determine the hfs anomaly, high precision measurements are required for both the magnetic dipole hfs interaction constant and the nuclear g-factor in pairs of isotopes.

Formalisms for calculation of the Bohr-Weisskopf effect with different nuclear models are summarized in ref.[5].

2.2 Proposed experiments

Alkali atoms are particularly suitable for the observations because the valence electron has a non-zero probability to penetrate the nucleus, the properties of which are probed. An extensive series of measurements done earlier at ISOLDE by laser and rf spectroscopy[6] indicate that the hfs anomalies in cesium would be of much interest. These experiments yielded the nuclear spins and the hyperfine structure separations $\Delta\nu$, which are related to the magnetic dipole hfs interaction constants by

$$\Delta\nu = a(I+1/2). \tag{5}$$

The nuclear moments which were obtained, either by (1) or directly from a measured g_I-factor, are not adequate to determine ε.

3 Experimental method

3.1 Principles

As stated above, the Bohr-Weisskopf effect measurement requires precise determinations of a and g_I. This is achieved with use of magnetic resonance transitions between hfs levels or magnetic sublevels of the ground atomic state. Fig. 1 shows a typical energy level diagram of an alkali atom in an external magnetic field. F is the total angular momentum quantum number, where $\mathbf{F} = \mathbf{I} + \mathbf{J}$, and $\mathbf{J}$ is the electron angular momentum. The allowed rf transitions are given by the selection rules $\Delta F = 0, \pm 1, \Delta m_F = 0, \pm 1$. The determination of a requires the measurement of the ($\mathrm{F}^+ = \mathrm{I} + 1/2$) - ($\mathrm{F}^- = \mathrm{I} - 1/2$) transitions in zero field. As detailed in sec. 4.2 and given by (8), g_I can be obtained by the difference of two transition frequencies at relatively high fields.

High resolution and sensitivity are required of the atomic beam apparatus shown schematically in fig. 2. The atomic beam is first polarized with the use of an optical pumping method: light from a laser diode, frequency tuned to the resonant transition $(^2S_{1/2}, F^+ = I+1/2) \rightarrow (^2P_{3/2}, F' = I+1/2)$ transfers the population of F^+ to the other hyperfine level $F^- = I - 1/2$ of the ground $^2S_{1/2}$ state. The atomic beam then crosses an

interaction region, described below, whose main effect is to induce a depolarization of the beam.

Finally, the depolarization (i.e. repopulation of F^+, empty after the optical pumping) is analyzed either with the use of a six-pole magnet, the property of which is to focus only atoms with $m_J = +1/2$ onto a detector, or by observing the fluorescence of the atomic beam excited by the same laser light as the one used for the polarization. This second method, has been used advantageously in preliminary experiments on stable atoms (see fig. 4).

The measurement of the magnetic dipole interaction constant a by this experimental method is straightforward: in the interaction region, a simple rf loop allows, when at resonance, the excitation of the hyperfine transition $F^- \rightarrow F^+$, which leads to a population of the F^+ level, and consequently a detectable signal. Such measurements were already done successfully earlier. [7]

The measurement of g_I is much more complex; for this we use the triple loop technique which is explained in more detail in sec. 4.2. Its principle is the following: the interaction region is composed of three separated magnetic field zones, successively A, C, B, in which three rf loops allow excitation of transitions between hfs levels and magnetic sublevels (see figs. 1,2). The rf in A acts on the atoms as a "$\pi pulse$" excitation to populate efficiently a single, well defined sublevel of the F^+ manifold (i.e. $m_F = 0$); the excitation in B is identical so that it cancels the effect of the first excitation. No change will thus be observed on the signal under the combined effect of these two excitations: they just provide the population of the desired level in the C region where a third rf loop (or for better resolution a *Ramsey loops* system) permits the excitation of the transition to be measured. At resonance, the populations of the different sublevels will be modified, leading to a detectable signal.

A ten percent accuracy in the measurement of a 0.1 percent hfs anomaly (the order of magnitude expected in our studies) indicates that the errors in the individual quantities appearing in (3) should be less than a part in 10^4. This is easily achievable for the hfs separations $\Delta\nu$ (typically several gigahertz), but not in the measurement of g_I. With the goal of this precision, or better, while retaining the sensitivity of the apparatus described in ref. [7], we had to devote a major effort to obtain a suitable magnetic resonance zone.

The accuracy in the determination of the resonance frequency depends on the line width and the signal-to-noise ratio. The former depends on the interaction time of the atom with the rf field and the homogeneity of the magnetic field in the interaction region. The latter depends on the effective solid angle of the apparatus. Besides these two well known requirements, the precision in the measurements of g_I increases with the magnetic field strength. With these considerations in mind, we have optimized the ABMR apparatus, in particular the magnet and rf loop systems, and have adopted the triple loop technique [8] with which g_I is measured at much higher fields than in the classical *field independent doublet* method.[9] Furthermore, this method is applicable to I = 1, which is the case of a number of isotopes which we intend to measure, and for which the *field independent doublet method* fails.

3.2 Atomic beam production

In test experiments, atomic beams of stable alkalis (potassium, rubidium, cesium) are produced by a conventional oven heated to $\sim 200^0 C$. A second oven for a reference beam of stable atoms, located in the vicinity of the first one, is installed to allow the calibration of magnetic field strengths for the *on-line* work. It also permits preliminary

tests of the apparatus before the *on-line* work. Collimation of the atomic beam is achieved with the use of cooled diaphragms.

3.3 Magnets

The triple loop method requires three homogeneous magnetic fields: A and B operating at low fields, and C, located between A and B, operating at a high field for g_I measurements (see fig. 2). To have the maximum effective solid angle for the transmission of the atomic beam apparatus, the A, B and C magnets have to be as close as possible to each other. On the other hand, in order to avoid the deterioration of homogeneity caused by stray fields, the A, B and C magnets have to be separated as far as possible. In this apparatus a compromise has been found with pole pieces of the A and B magnets located 7cm apart from both ends of the pole pieces of the C magnet. These pole pieces are mounted in the vacuum chamber.

3.3.1 C magnet

The C magnet has been designed to give the desired homogeneous magnetic field. It has a 25-mm gap, with pole pieces 20 cm high and 30 cm long. The pole faces are polished to an optical quality and spaced with quartz blocks to give a gap parallel to within a few microns. The field calibration, as described in sec. 4.3, has shown the homogeneity to be about 5×10^{-6} at 0.65T in the central region where the rf loops are located. The magnet current is supplied by a power supply with a long term stability better than 3×10^{-6} (Dan Fysik MPS858 system 8000, 100A, 47V). A current of 62A gives a magnetic field of 0.7T. This field is monitored by a NMR magnetometer.[10] The field strength is given by the NMR resonant frequency $\nu_H(\Gamma_{p,H_2O} = 4257.608(12)Hz/G)$. To stabilize the C field, an external rf generator is set to the frequency ν_0 corresponding to a desired field strength. The rf generator ouput is then applied to the NMR detector. The error voltage which is proportional to the difference between ν_0 and $\nu_H(t)$ is converted by feedback electronics into a current which is fed to a correcting coil on the C magnet to induce the ΔB field required for the stabilization. In this way the field could be stabilized at the level of 2×10^{-6} for many hours.

3.3.2 A and B magnets

The A and B magnets are of much simpler design, 25-mm gap, 9×4-cm pole pieces. A field mapping has shown the homogeneity to be about 10^{-2}. The current in the A and B magnets is supplied by regulated power supplies (2A, 15V) with 10^{-3} stability. A current of 1A gives a magnetic field of about 300G. The A and B magnets are excited to produce a field in a direction opposite to the one of the C magnet so as to compensate the stray field from the latter when g_I is measured. The fields are monitored with a Hall probe which can be inserted permanently near the A and B loops.

3.3.3 Six-pole magnet

This focussing magnet has been described in ref.[11]. A current of 120A creates a magnetic field of 1T at the pole tips. To meet the solid angle requirements in this apparatus, the pole tips have been reshaped to a length of 45cm and the entrance and exit apertures to a diameter of 14mm.

All these magnets were constructed at Chalmers University of Technology and Uppsala University.

3.4 Radiofrequency system

Schematic drawings of the rf loops are shown in fig. 3. These are essentially shorted terminations of a coaxial tube of copper. In the A and B regions we induce $\Delta m_F = 0$ auxiliary transitions, so that the loops have a structure to produce the necessary rf magnetic field parallel to the static one (fig. 3a). On the other hand, in the C region, as we induce $\Delta m_F = 1$ transitions, the loops are made so as to produce an rf field perpendicular to the static one (fig. 3b). As mentioned earlier, to increase the transit time, i.e. to get narrower line widths, two 2-cm long loops separated by 2 cm are used in the C region to produce a *Ramsey pattern* transition.[12] In order to achieve the required large acceptance of the apparatus, the apertures of the A and B loops were made wide, 1.2×1.2 cm^2. The width of the C loops is 9 mm.

Radiofrequencies up to 1GHz are produced by several generators: Rohde & Schwarz SMS (0.4-1040MHz) and Marconi Instr. 2022C (0.01-1000MHz). With frequency doublers, this range could be extended to 4GHz. Higher frequencies are obtained from the generator Gigatronics 7100 (0.01- 20GHz). The rf frequency and output level can be controlled automatically by an IBM-PC with an IEEE-488 (GPIB) bus interface. The radiofrequency is counted in specific cases with the use of a CW microwave counter, EIP Microwave 625A. As illustrated in sec. 4.3, rf power of the order of 1W may be needed, so that we used different amplifiers according to the required frequency ranges, Nuclétudes S.A. (SCD) ARS series, and Avantek APT series. The rf power was measured with a Marconi Instr. 6960A power meter, with attenuators used when necessary.

3.5 Laser system

The potassium, rubidium and cesium atomic D lines all lie in a wavelength region accessible to available diode lasers. The single mode diode lasers (Mitsubishi ML series) which we use are selected ones, with wavelengths emitted at room temperature near the D_2 lines. Stable emission in a single mode was obtained by controlling the temperature of the diode holder to 10^{-3} degrees and the current of about 40 mA to 1μA. The emitted intensity of a few mW is sufficient to produce strong optical pumping. The laser frequency is locked with the use of a feedback system to a stable Fabry- Perot cavity, as shown in fig. 4.

3.6 Detection system

As noted in sec. 3.1, the polarization of the atomic beam can be analyzed with use of the six-pole magnet.[7] The atoms are then ionized by surface ionization on a hot tantalum tube, passed through a mass spectrometer, and counted, as described in detail in earlier on-line work. [13] Detection by the simpler laser induced fluorescence (LIF), which we used in the test experiments with stable isotopes (see fig. 4), may also be possible for the on-line studies. The laser beam is split into two parts. The major one is used to polarize the atomic beam by optical pumping. The other one allows us to analyze the atomic beam polarization after the rf interaction region by detecting, with use of a photomultiplier, the induced fluorescence. The anode current of the photomultiplier is amplified and fed via an ADC board into the computer, and is also monitored on a chart recorder. We have obtained the same results when we use the six-pole magnet for the atomic beam polarization analysis. A more efficient scheme for fluorescence detection is to use, after the third rf zone, the optical pumping-free transition ($F^+ = I + 1/2 \rightarrow F' = I + 3/2$) to probe the population of F^+. This makes possible the multiple re-excitation of a single

atom (up to $\sim 10^8$ times for alkali atoms), thereby increasing by many orders of magnitude the available signal.

4 Measurements on stable alkalis

Test experiments have been done on stable ^{39}K, ^{85}Rb and ^{87}Rb. These isotopes were chosen because their hfs separations are similar to those of the I=1 cesium isotopes to be investigated. Furthermore, since precise values of g_J, g_I and $\Delta\nu$ are known for them[14][15][16][17], they can serve to test the performance of the apparatus.

Here we explain the present method of the measurements for the case of ^{39}K, with I=3/2.

4.1 $\Delta\nu$ measurement

In fig. 1 we show the energy level diagram applicable to ^{39}K in a magnetic field. The ground electronic $^2S_{1/2}$ state is split into two hyperfine levels with F^+=2 and F^-=1. The excited $^2P_{3/2}$ state is split into four hfs levels, F'=0, 1, 2 and 3. The optical excitation from the $^2S_{1/2}$ F^+=2 sublevels to the $^2P_{3/2}$ F'=2 level transfers the population from F^+=2 sublevels to those of F^-=1, thus producing a beam polarization. The energy levels as a function of the magnetic field B are given by the Breit-Rabi formula[12],

$$W(F, m_F) = -\frac{h\Delta\nu}{2I(I+1)} + g_I\mu_B B m_F \pm \frac{h\Delta\nu}{2}\sqrt{1 + \frac{4m_F}{2I+1}x + x^2}, \qquad (6)$$

where the field parameter x is defined by

$$x = (g_J - g_I)\mu_B B/h\Delta\nu. \qquad (7)$$

The electronic and nuclear g-factors, g_J and g_I, are expressed in Bohr magnetons, with $g_J = -\mu_J/J$ and $g_I = -\mu_I/I$. The $\pm$ signs refer to the hyperfine levels $F^{\pm}$.

In fig. 5 we show a spectrum observed for a low value of x with the present apparatus using one of the rf loops in the C region. The central dip in the *field independent* transition, $\Delta F = \pm 1, m_F = 0 \rightarrow m_F = 0$ (labelled by $\sigma 2$) appears as a result of effective *Ramsey transitions*, the phases of which differ by π, as described in ref.[7]. We can thus readily determine directly the hfs separation within an error of $\pm$1kHz.

4.2 Measurement of g_I by the triple resonance method

The triple resonance technique has been devised as a method for obtaining the nuclear magnetic g-factor directly by observing $\Delta m_J = 0, \Delta m_I = \pm 1$ transitions.[8] It is applicable to atomic nuclei with spins larger than 1/2. The principle of this technique has been given in sec. 3.1. Here we describe the triple loop technique in more detail in the case of ^{39}K (I=3/2) (fig. 1). We illustrate it with use of the relative signal levels shown in fig. 6.

We consider the three-level system applicable to the present triple resonance experiment, fig. 7. The population of F^+=2 sublevels is transferred to F^-=1 sublevels equally by the optical pumping. We take the population of each F^-=1 sublevel to be one unit before the rf excitation, whereas the population of the F^+=2 sublevels is zero. First suppose that in the loop A we induce the transition ν_A between (F=2, m_F=0) and (1,0) sublevels with the transition probability a. This leads to an increase of light induced fluorescence (LIF) proportional to a (fig. 7-b), since we have transferred atoms from a non-focussing (m_J = -1/2) to a focussing (m_J = + 1/2) state. Similarly, with rf in loop B only, we induce the

same transition ν_B with probability b. Thus we can select values of a and b so as to give the maximum increase of observed LIF signal. When both loops A and B are excited, the resulting population of the (2,0) level will be proportional to $a+b(1-a)-ba$. The first term results from the first transition ν_A, the second and third terms account for the population transferred from (1,0) to (2,0) and the depleting one from (2,0) to (1,0) caused by the following transition ν_B (fig. 7-c). It is seen in fig. 8 that this relation reproduces the observed rf power dependence of the signals. Next suppose that we induce the transition $\nu_1(2,0) \leftrightarrow (2,1)$,with probability c, between the transitions ν_A and ν_B. The resulting population in the F=2 sublevels is expressed as one proportional to $a+b(1-2a)+abc$ (fig. 7-f). For the case of fig. 6, one finds $a=b=0.99$, and $c=0.72$.

A similar resonance is obtained for the transition $\nu_2(1,0) \leftrightarrow (1,1)$, with an identical sequence as described above.

Finally, one can find readily the frequency separation $\delta\nu$ from the Breit-Rabi formula,

$$\delta\nu = \nu_1 - \nu_2 = 2g_I\mu_B B_C/h. \tag{8}$$

We can thus obtain g_I directly from $\delta\nu$ and the known value of the magnetic field B_C. In the present case with I=3/2, we can obtain the same quantity from another pair of transitions, $\nu_1'(2,0) \leftrightarrow (2,-1)$ and $\nu_2'(1,0) \leftrightarrow (1,-1)$.

The transitions used in the triple resonance method are usually less field dependent at higher fields, scaled by the parameter x. For an atom with larger hfs separation, the field dependence of the resonance frequencies is relatively larger, so that field inhomogeneities become more important and contribute to a loss of accuracy in the measurements.

4.3 Procedure and results

The rf power needed to obtain a high transition probability in the loops A and B depends critically on the homogeneity achieved in these fields and the efficiency of the loops. In this apparatus, because of the mutual stray fields of the A, B and C magnets, the best conditions are sought by systematic trials of the combination of these fields. Even under these conditions, the line width of the A and B transitions is quite large, and thus, to saturate the transition, about 500 mW rf power is required for the A or B loops (see fig. 8).

The transition probability of $\Delta m_J = 0, \Delta m_I = \pm 1$ transitions (i.e., the transitions for measuring g_I in the C field for large x), depends on the value of the magnetic field. It is roughly proportional to $1/x^2$.[18] Much more rf power was thus required to observe the resonances for ^{39}K ($\sim 500\,mW, x = 39.45$) than for ^{85,87}Rb isotopes ($\sim 20mW, x = 6.00$ and 2.67, respectively) at 0.65 T.

In order to deduce the g_I factor with the desired accuracy, the average value of B_C over the *Ramsey loops* must also be similarly well known. The value B_{NMR} seen by the NMR probe is found to be different from the true magnetic field B_{atom} seen by the atoms in the *Ramsey loops*. The relative difference is 1×10^{-4}. To measure B_{atom}, a beam of ^{133}Cs or ^{87}Rb atoms from the same oven or the reference oven was used. The highly field-dependent transition (F^+, -I-1/2) $\leftrightarrow$ (F^-, -I+1/2) is measured with each loop in turn with the use of LIF detection. By adjusting the A and B (stray) fields, the two resonance frequencies can be set equal to better than one part in 10^6. One then determines the correction needed to obtain B_{atom} from B_{NMR}. We have also measured g_I after reversing the direction of the static magnetic field to eliminate the so-called *Millman effect*[12]: this was found to be negligible for rubidium isotopes within the present experimental uncertainty.

As mentioned in sec. 3.1, narrow line widths are necessary to obtain sufficiently precise measurements. At first, we used a 3-cm long single loop in the C region. It gave resonance widths of $\sim$ 6 to 7kHz, limited by the transit time through the rf loop. To get better precision, the *Ramsey loop* system is used to achieve a line width of 3 to 5 kHz, depending on the strength of the rf field.

A typical resonance curve is shown in fig. 9. The rf frequency was scanned in 0.4 kHz steps, and the time required to record one resonance was a few minutes. Most of the error arises from the uncertainty in the determination of the central frequency, which is obtained, by the method described in ref. [15], to a precision of almost one percent of the resonance line width.

The same procedure was used with ^{85}Rb and ^{87}Rb to measure the hfs separation $\Delta\nu$ at low fields ($\sim 0.1G$) with a single loop, and the nuclear g-factor at high fields ($\sim 0.65T$) with the triple resonance method.

The results for $\Delta\nu$ and g_I are given in table I. We also show for comparison previously measured values. Depending on the separation $\delta\nu$, g_I was measured with an accuracy of better than 8×10^{-5}. The quoted error margins represent the spread of the measured values. We obtained easily an accuracy of better than 10^{-6} for the hfs separations $\Delta\nu$. From the measurements of ^{85}Rb and ^{87}Rb, the hyperfine anomaly is evaluated to be $^{85}\Delta^{87} = 0.00356(9)$. This value is to be compared with the most precise value 0.003514(2), which was obtained in a dedicated experiment[17] in which wall-coated cells filled with ^{85,87}Rb were used. A similar setup would be very difficult to implement on line for study of long chains of radioactive isotopes. In contradistinction, the apparatus that we describe here is well adapted for this type of work, although the accuracy obtained is smaller. Nevertheless a and g_I have been measured with an accuracy of the order of 10^{-5}, which is better than the goal of 10^{-4} which we set in sec. 3.1.

5 Conclusion

In the on-line case the conditions are of course different, in particular the number of atoms is much less than in a beam of stable isotopes. We recall that in the previous setup[7] the rf resonances, induced at low fields to measure the hfs of rubidium isotopes, had a width of $\sim$50kHz, an order of magnitude larger than in this apparatus. Nevertheless an uncertainty of 4kHz (about one tenth of the line width) was obtained in the case of ^{76}Rb, produced at a rate of $2 \times 10^6/s$. For the cesium isotopes to be investigated the production rate is expected to be more than $10^9/s$. If the resonance frequencies are measured to a conservative 1kHz, it is seen that such precision is adequate to measure the hfs anomalies to about 10 percent or better. The apparatus is presently being set up at the new ISOLDE facility at the CERN PS Booster (PSB ISOLDE) for the on-line measurements of a sequence of radioactive cesium isotopes.

Acknowledgments

One of us (T.M.) heartily thanks the Yamada Science Foundation in Japan and the C.N.R.S. in France for financial support of the long term stay at the Laboratoire Aimé Cotton, Orsay. Another (H.H.S.) is grateful to Dr. H. Haas for stimulating discussions and to the CERN ISOLDE group for their hospitality; he also thanks Dr. C. Bréchignac and the staff of the Laboratoire Aimé Cotton for their kind reception. The following acknowledgments for support are made by: O.Redi and H.H.Stroke to the U.S. National Science Foundation in part under grants NSF-INT8815310 and NSF-ECS8819352; C.Ekström, M.

Gustafsson, I. Lindgren, T. Nilsson, J. Persson, and I. Ragnarsson to the Swedish Natural Science Research Council; T.T. Inamura, S. Matsuki, and T. Nomura for the Grant-in-Aid for International Scientific Joint Research from the Ministry of Education, Science and Culture in Japan.

References

[1] E.W. Otten, in *Treatise on Heavy Ion Physics*, Vol. 8 Nuclei Far From Stability, edited by D.A. Bromley (Plenum, New York, 1988), p. 517.

[2] A. Bohr and V.F. Weisskopf, Phys. Rev. **77** (1950) 94.

[3] V.A. Dzuba, V.V. Flambaum, A. Ya. Kraftmakher, O.P. Sushkov, Phys. Lett. A **142** (1989) 373; A.C. Hartley and A.M. Mårtensson-Pendrill, Z. Phys. D **15** (1990) 309; S.A. Blundell, W.R. Johnson, and J. Sapirstein, Phys. Rev. A **43** (1991) 3407, and references therein.

[4] H.J. Rosenberg and H.H. Stroke, Phys. Rev. A**5** (1972) 1992.

[5] S. Büttgenbach, Hyperfine Interactions **20** (1984) 1.

[6] C. Ekström, S. Ingelman, G. Wannberg, M. Skarstad, Nucl. Phys. A **292** (1977) 144; C. Ekström, G. Wannberg, J. Heinemeier, Phys. Lett. **76B** (1978) 565; C. Ekström, C. Robertsson, G. Wannberg, J. Heinemeier, Phys. Scr. **19** (1979) 516; G. Huber, C. Thibault, F. Touchard, S. Büttgenbach, R. Klapisch, M. de Saint Simon, H.T. Duong, P. Jacquinot, P. Juncar, S. Liberman, P. Pillet, J. Pinard, J.L. Vialle, A. Pesnelle, Phys. Rev. Lett. **41** (1978) 459 and Nucl. Phys. A **367** (1981) 1; B. Schinzler, W. Klempt, S.L. Kaufman, H. Lochmann, G. Moruzzi, R. Neugart, E.-W. Otten, J. Bonn, L. Von Reisky, K.P.C. Spath, J. Steinacher, and D. Weskott, Phys. Lett. **79B** (1978) 209.

[7] H.T. Duong, S. Liberman, J. Pinard, A. Coc, C. Thibault, F. Touchard, M. Carré, L. Lermé, J.L. Vialle, P. Juncar, S. Büttgenbach, A. Pesnelle, and the ISOLDE Collaboration, J. Phys. **47** (1986) 1903.

[8] G.K. Woodgate and P.G.H. Sandars, Nature **181** (1958) 1395; G.O. Brink and W.A. Nierenberg, J. Phys. Radium **19** (1958) 816.

[9] See, for example, H.H. Stroke, V. Jaccarino, D.S. Edmonds, Jr. and R. Weiss, Phys. Rev. **105** (1957) 590.

[10] K. Borer, Nucl. Instr. Methods **143** (1977) 203.

[11] C. Ekström, M. Olsmats and B. Wannberg, Nucl. Instr. Methods **103** (1972) 13.

[12] N.F. Ramsey, *Molecular Beams* (Oxford University Press, New York, 1956).

[13] G. Huber, F. Touchard, S. Büttgenbach, C. Thibault, R. Klapisch, H.T. Duong, S. Liberman, J. Pinard, J.L. Vialle, P. Juncar, P. Jacquinot, Phys. Rev. C **18** (1978) 2342; H.T. Duong, P. Juncar, S. Liberman, J. Pinard, J.L. Vialle, S. Büttgenbach, P. Guimbal, M. de Saint Simon, J.M. Serre, C. Thibault, F. Touchard, R. Klapisch, J. Phys. **43** (1982) 509.

[14] K.D. Böklen, W. Dankworth, E. Pitz, S. Penselin, Z. Phys. **200** (1967) 467.

[15] A. Beckmann, K.D. Böklen and D. Elke, Z. Phys. **270** (1974) 173.

[16] S. Penselin, T. Moran, V.W. Cohen and G. Winkler, Phys. Rev. **127** (1962) 524; B. Bederson and V. Jaccarino, Phys. Rev. **87** (1952) 228(A) and H.H. Stroke, R.J. Blin-Stoyle and V. Jaccarino, Phys. Rev. **123** (1961) 1326.

[17] C.W. White, W.M. Hughes, G.S. Hayne and H.G. Robinson, Phys. Rev. **174** (1968) 23.

[18] H.C. Torrey, Phys. Rev. **59** (1941) 293.

Table 1: Measurements of $\Delta\nu$ and g_I of ^{39}K, ^{85}Rb and ^{87}Rb.

atom	I	$\Delta\nu$[MHz] present work	$\Delta\nu$[MHz] prior work	$-g_I \times 10^4$ present work	$-g_I \times 10^4$ prior work
^{39}K	3/2	461.7198(2)	461.7197202(14)[a]	1.41935(11)	1.4193489(12)[a]
^{85}Rb	5/2	3035.7325(10)	3035.732439(5)[b]	2.93636(22)	2.936400(6)[c]
^{87}Rb	3/2	6834.6830(10)	6834.682614(3)[b]	9.95170(44)	9.951414(10)[c]

[a]ref.[15], [b]ref.[16], [c]ref.[17]

Figure Captions

1. Hfs energy levels in a magnetic field B for ^{39}K (I=3/2) in the ground $^2S_{1/2}$ state. Low field m_F and high field m_J, m_I quantum numbers are indicated, as are the transitions used for the triple resonance method and for the optical pumping via the excited $^2P_{3/2}$ state. The magnetic field parameter $x \propto B$.

2. Schematic of experimental setup of ABMR at ISOLDE.

3. Sketches of rf loops a) for *A*- and *B*- and b) for *C*- field transitions.

4. Schematic of the laser optical pumping, laser induced fluorescence detection of the triple resonance, and of the stabilization setup.

5. Spectrum of ^{39}K at low field for $\Delta F = \pm 1$ transitions ($\sigma \quad \Delta m = 0, \pi \quad \Delta m = \pm 1$). The signal was obtained by light induced fluorescence (LIF).

6. Typical LIF signal strengths with applications of the rf and light fields (see sec. 4.2). O.P. denotes optical pumping, and S_A, etc. the signals with the application of rf in loops *A*, etc.

7. Diagrams for illustrating level populations with application of rf in the three loops. The quantum numbers F, m_F of the magnetic sublevels are indicated in the parentheses. The transition probabilities are labelled by *a*, *b*, *c*. The dotted arrows (I) $\rightarrow$ (II) $\rightarrow$ (III) show the sequence corresponding to the application of rf to loops A and B. The sequence (I) $\rightarrow$ (IV) $\rightarrow$ (V) $\rightarrow$ (VI) gives the populations with the excitation of rf resonances in loops *A*, *C* and *B*.

8. Dependence on rf power of detected signals in ^{39}K (see, fig. 6).

9. Typical F=2, m_F=0 $\leftrightarrow$ F=2, m_F=1 resonance in ^{39}K obtained at 0.65T.

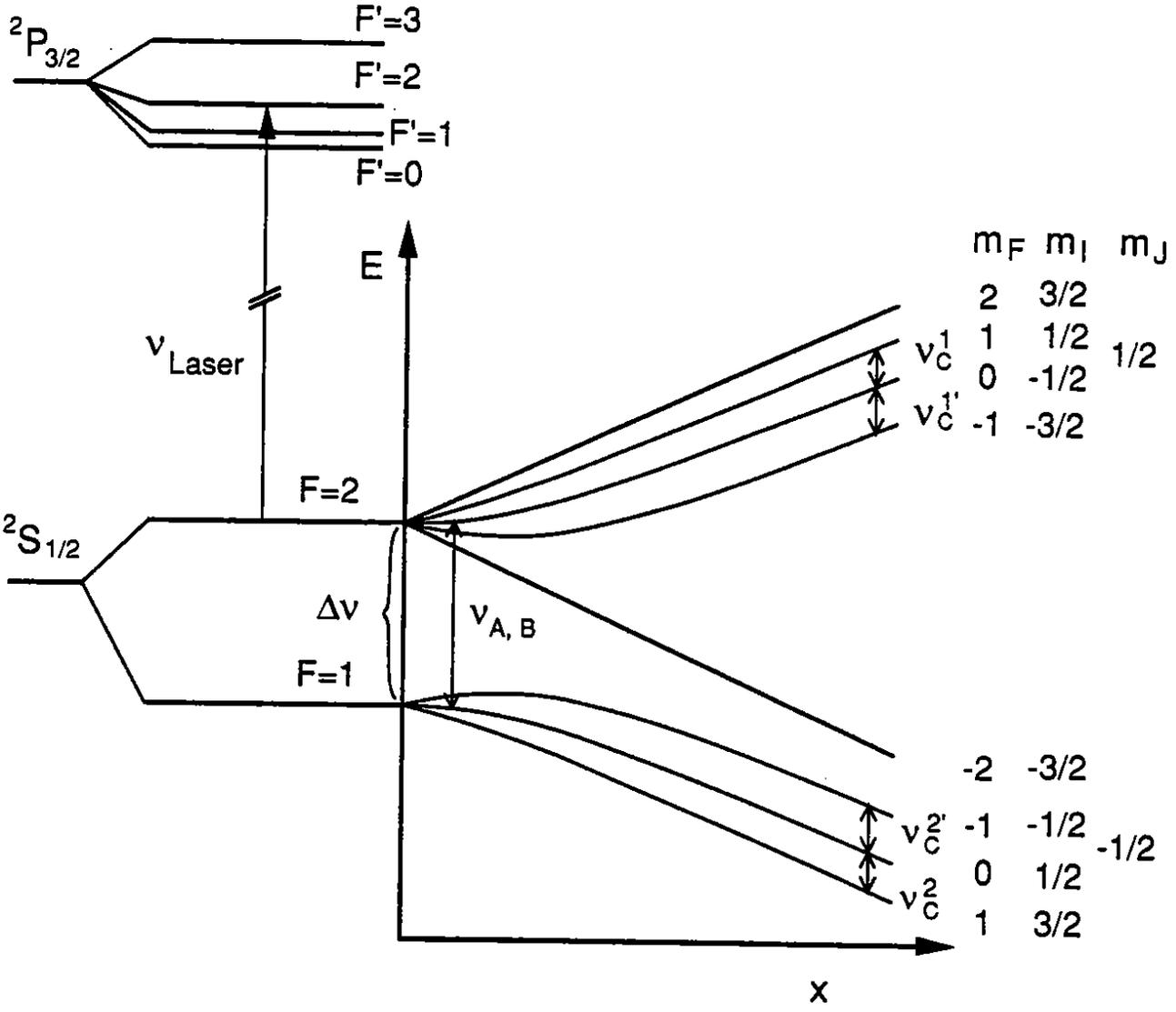
$^2P_{3/2}$
F'=3
F'=2
F'=1
F'=0
E
ν_{Laser}
F=2
$^2S_{1/2}$
$\Delta\nu$
$\nu_{A,B}$
F=1
m_F m_I m_J
2 3/2
ν_C^1 1 1/2 1/2
0 -1/2
$\nu_C^{1'}$ -1 -3/2
-2 -3/2
$\nu_C^{2'}$ -1 -1/2 -1/2
0 1/2
ν_C^2 1 3/2
x

Fig. 1

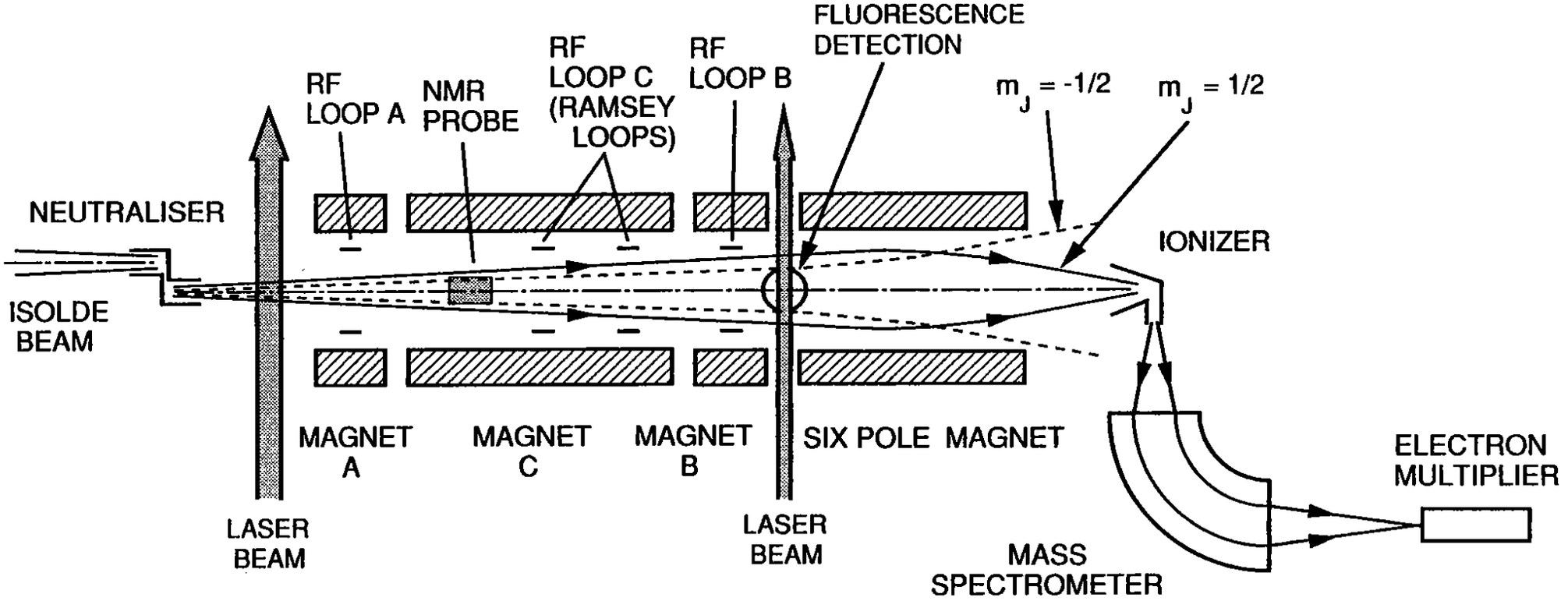
FLUORESCENCE
DETECTION
RF
LOOP C
(RAMSEY
LOOPS)
RF
LOOP B
RF
LOOP A
NMR
PROBE
$m_J = -1/2$
$m_J = 1/2$
NEUTRALISER
IONIZER
ISOLDE
BEAM
MAGNET
A
MAGNET
C
MAGNET
B
SIX POLE MAGNET
ELECTRON
MULTIPLIER
LASER
BEAM
LASER
BEAM
MASS
SPECTROMETER

Fig. 2

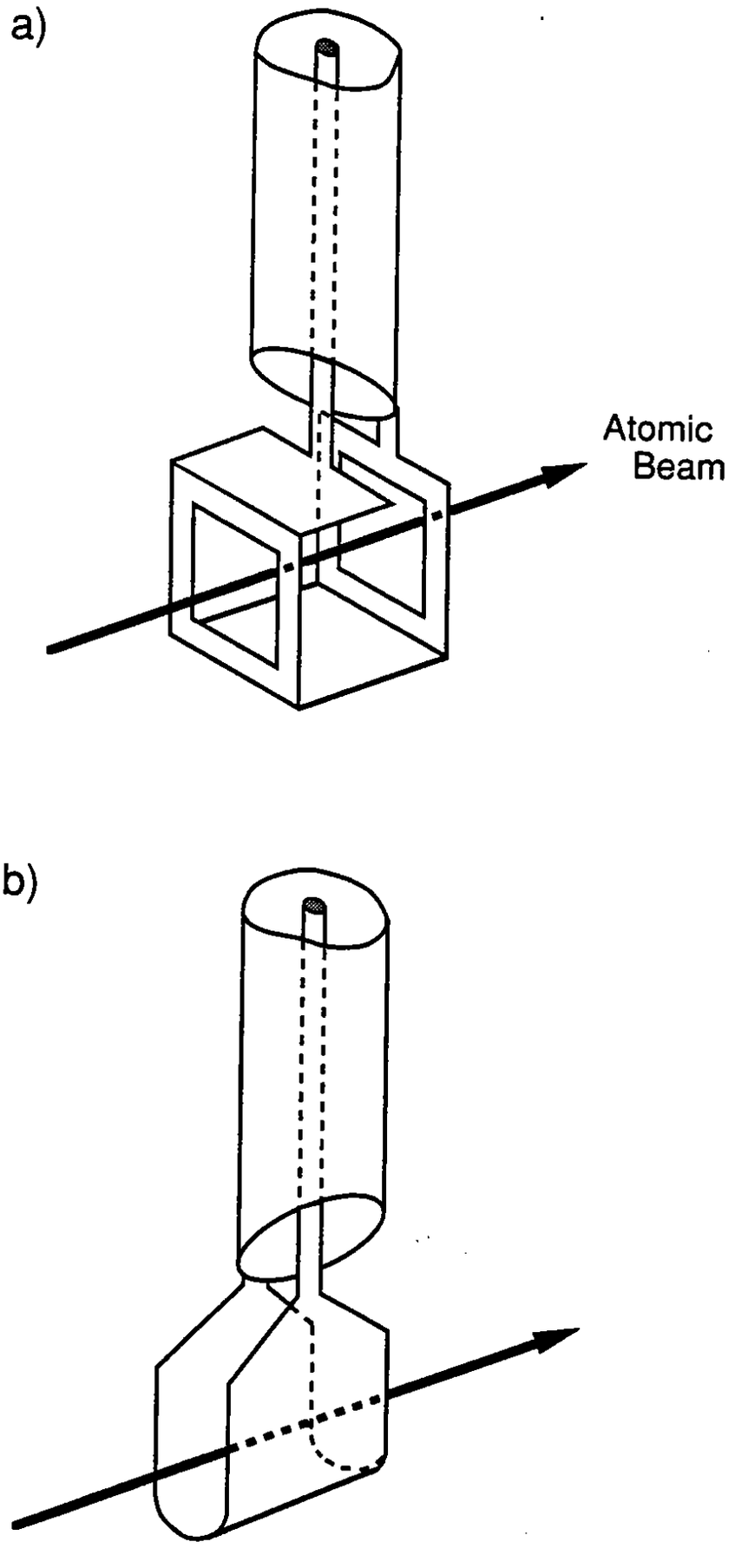

Fig. 3

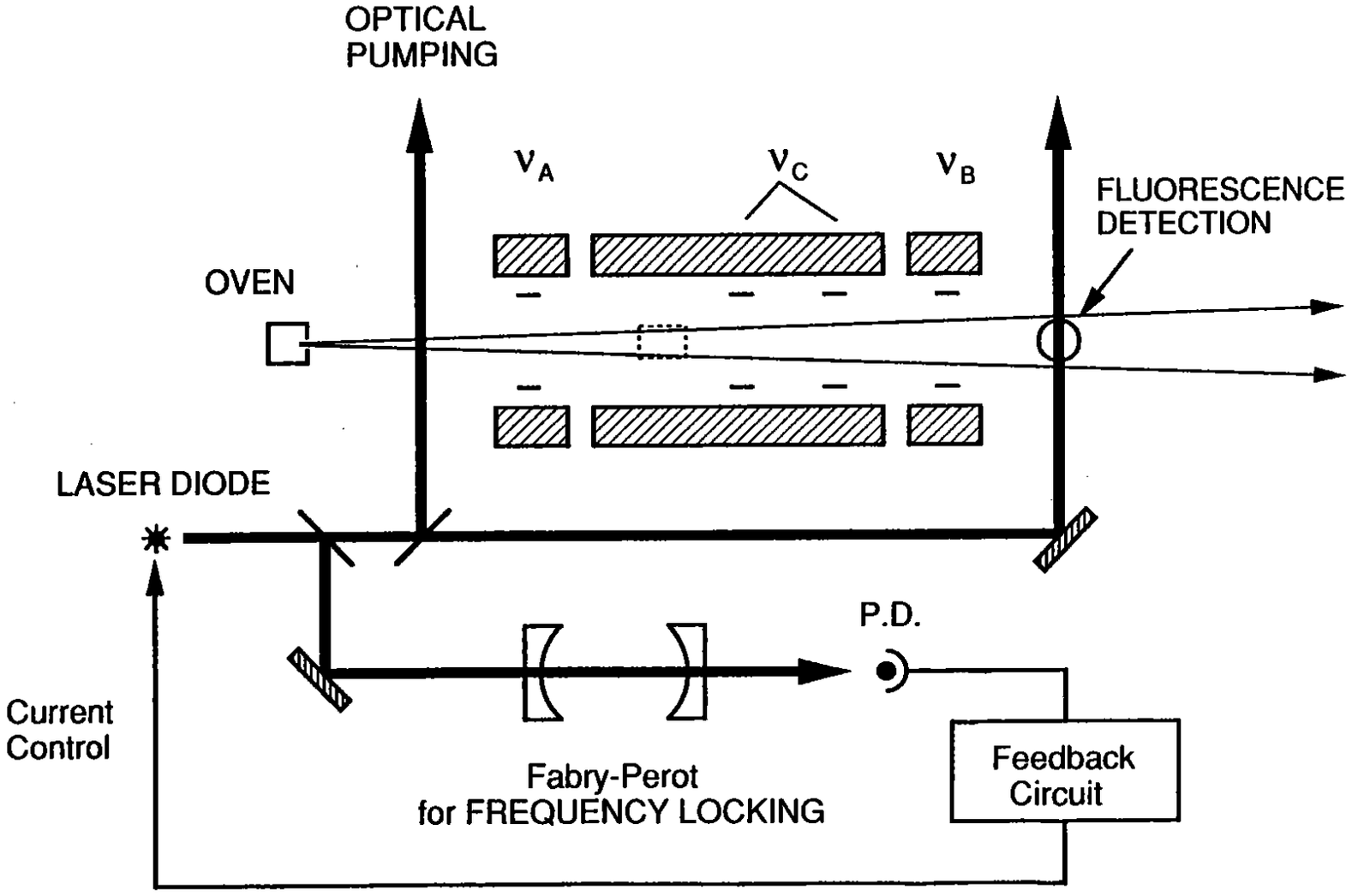
OPTICAL
PUMPING
ν_A
ν_C
ν_B
FLUORESCENCE
DETECTION
OVEN
LASER DIODE
P.D.
Current
Control
Fabry-Perot
for FREQUENCY LOCKING
Feedback
Circuit

Fig. 4

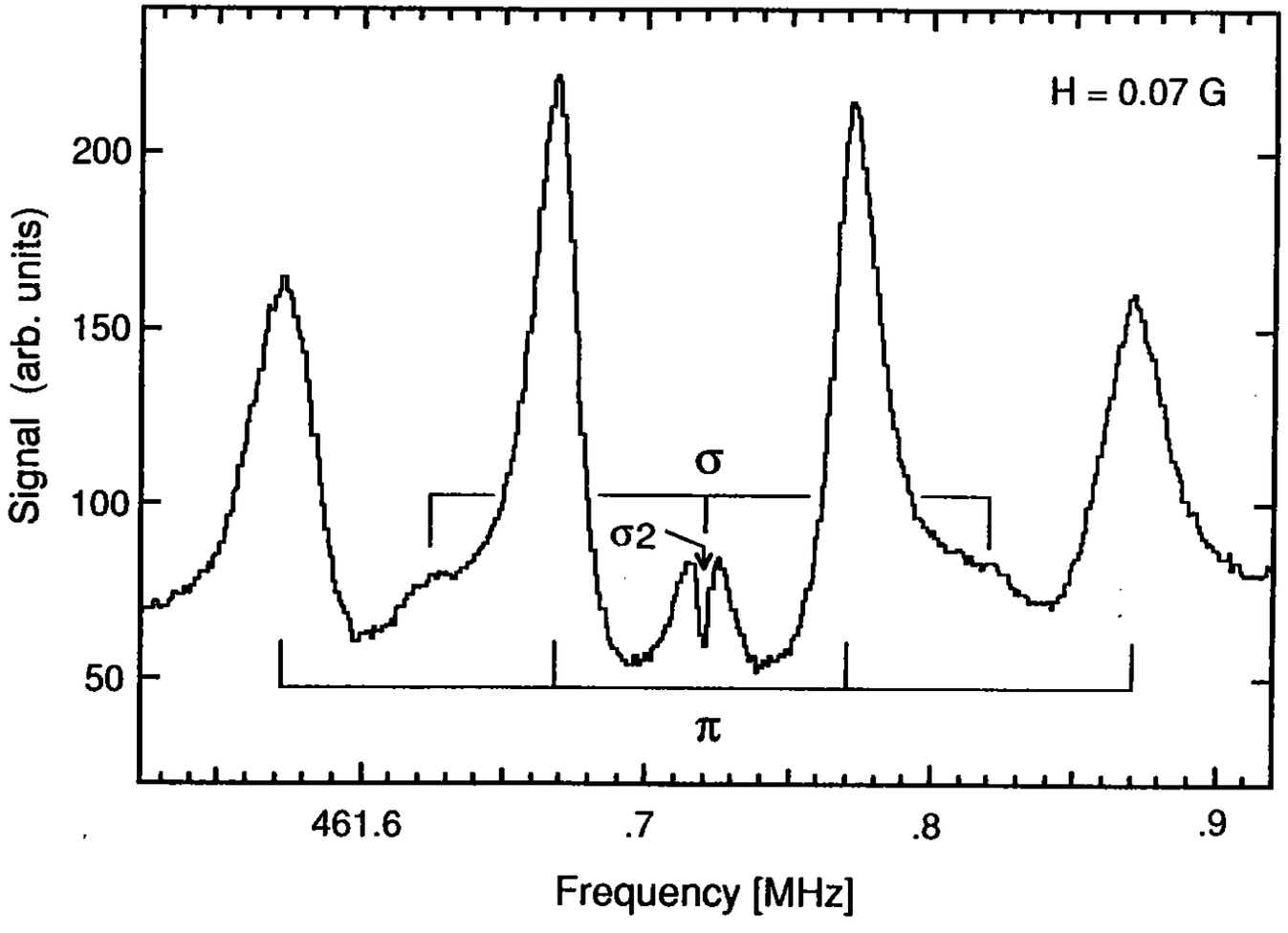
H = 0.07 G
Signal (arb. units)
200
150
100
50
σ
σ2
π
461.6
.7
.8
.9
Frequency [MHz]

Fig. 5

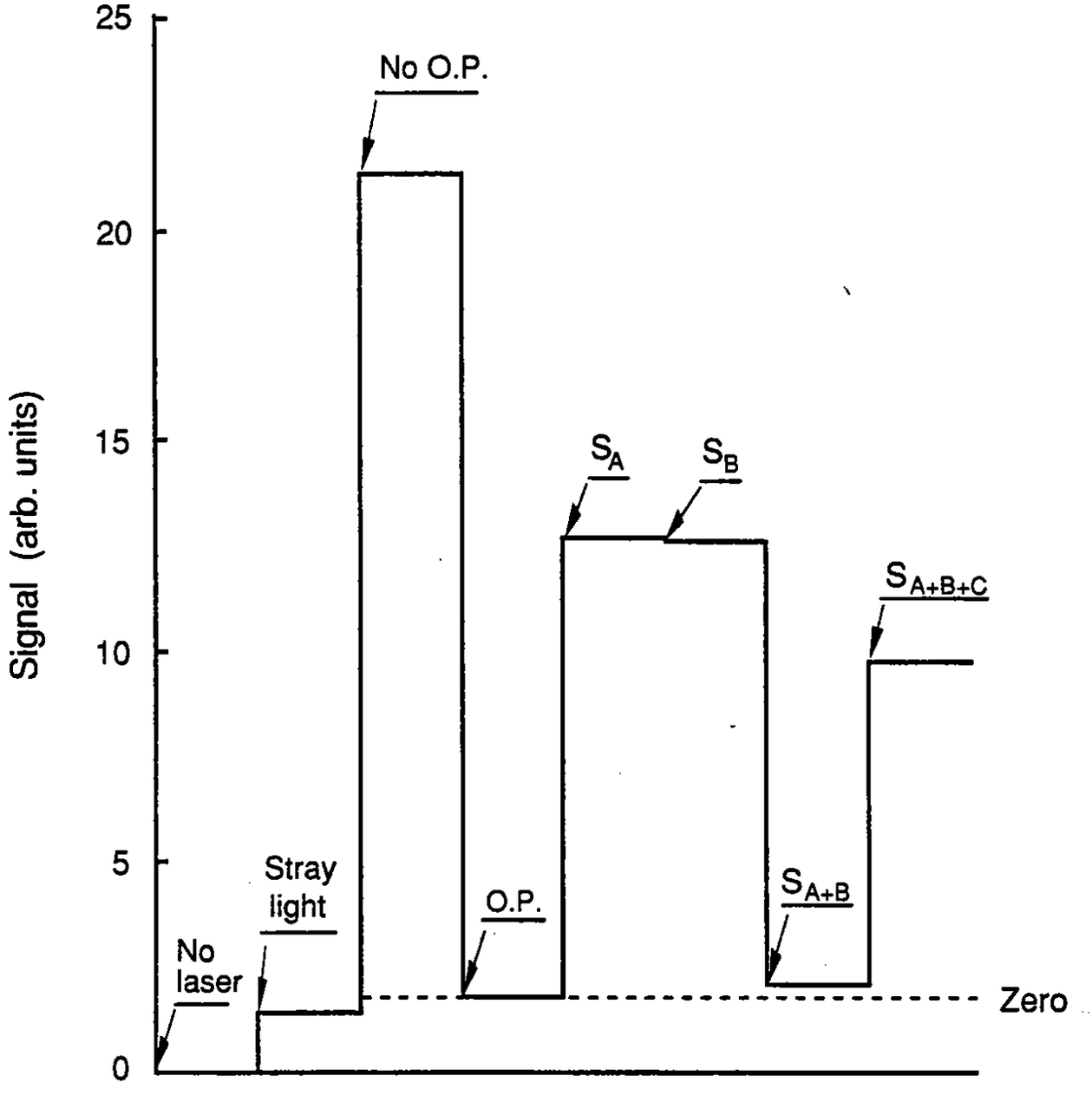
25
20
15
10
5
0
Signal (arb. units)
No O.P.
S_A
S_B
S_{A+B+C}
Stray light
O.P.
S_{A+B}
No laser
Zero

Fig. 6

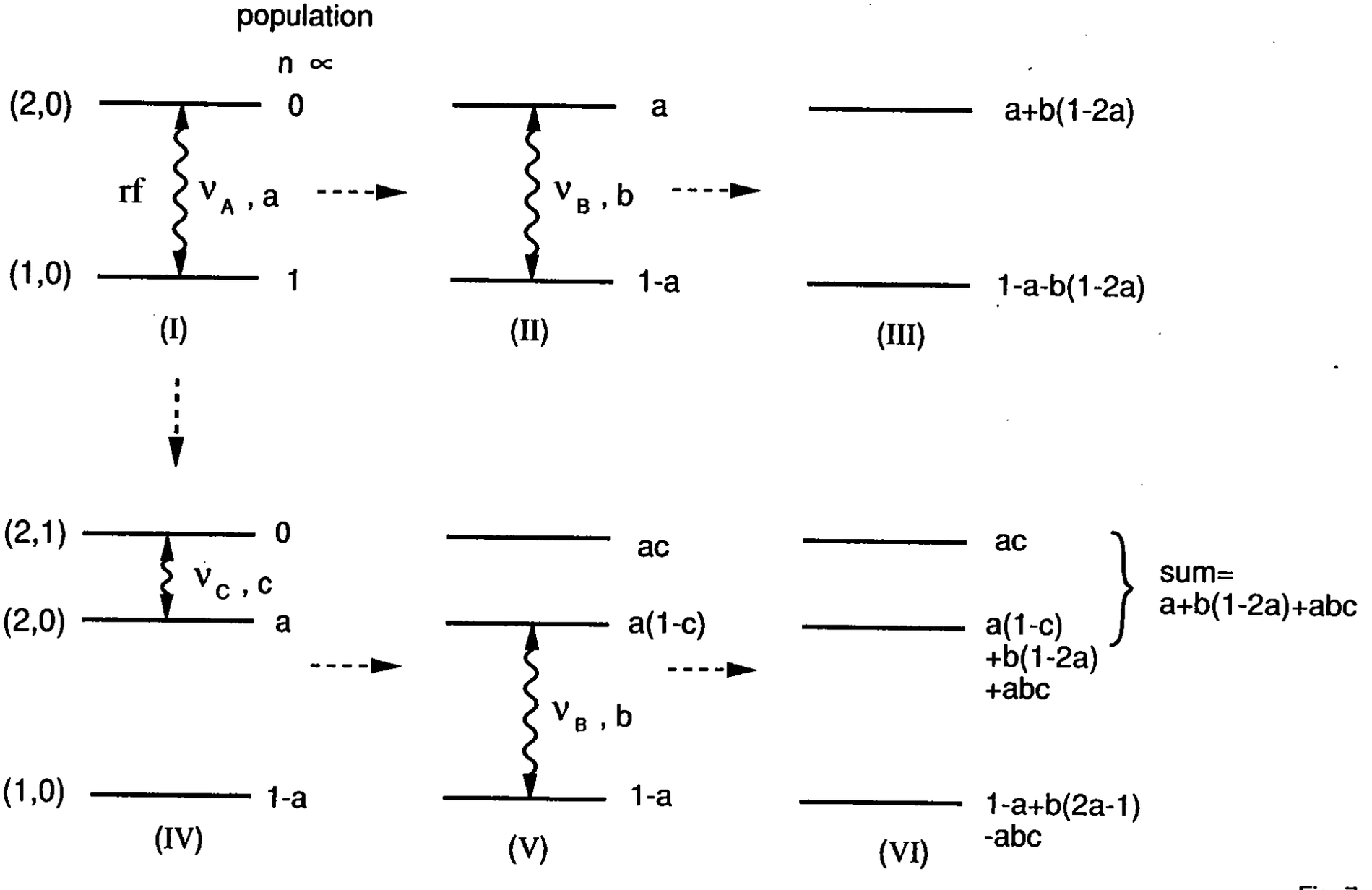
population
n ∝
(2,0)
0
rf
ν_A , a
(1,0)
1
(I)
a
ν_B , b
1-a
(II)
a+b(1-2a)
1-a-b(1-2a)
(III)
(2,1)
0
ν_C , c
(2,0)
a
(IV)
ac
a(1-c)
ν_B , b
1-a
(V)
ac
a(1-c)
+b(1-2a)
+abc
sum=
a+b(1-2a)+abc
1-a+b(2a-1)
-abc
(VI)

Fig. 7

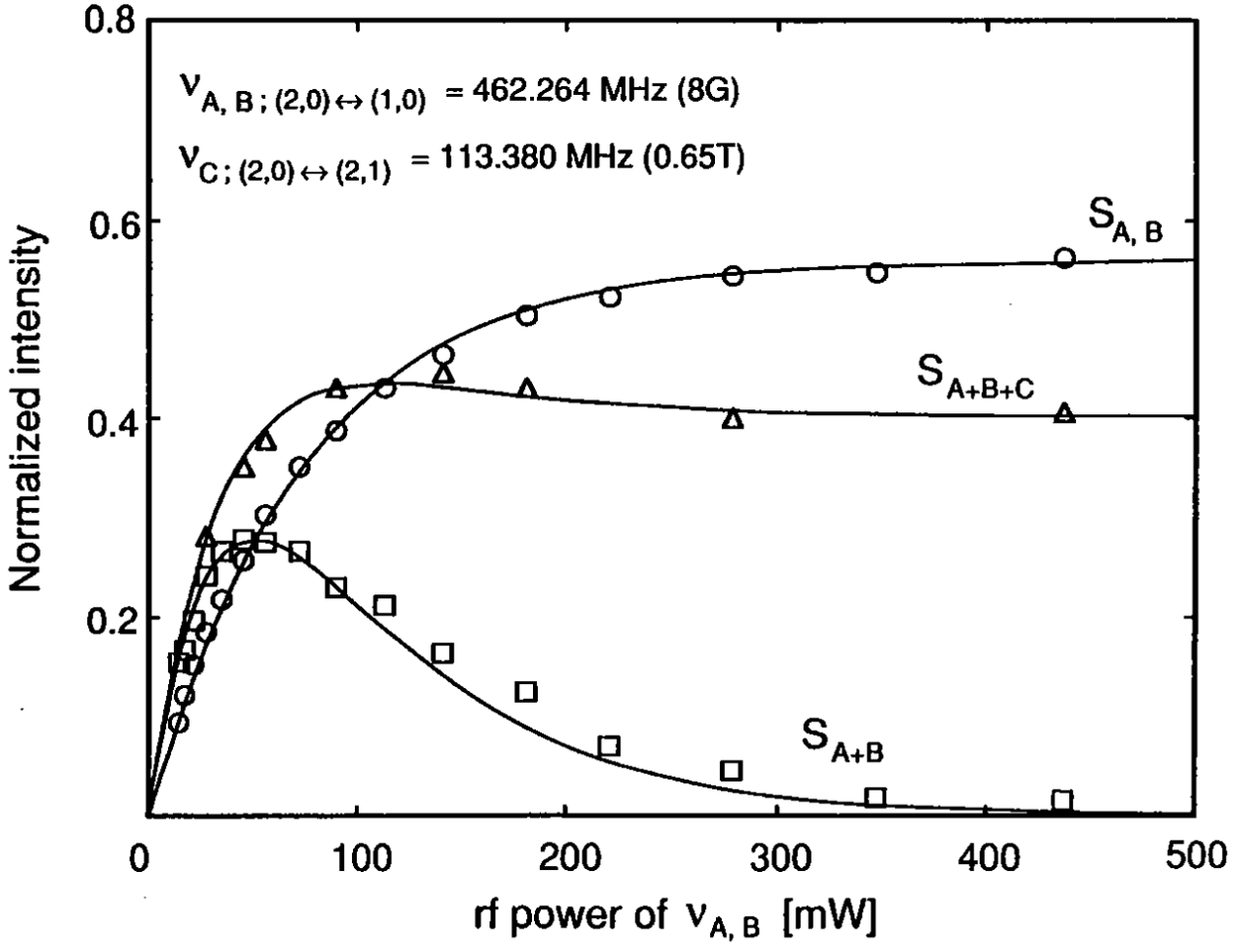
0.8
0.6
0.4
0.2
0
100
200
300
400
500
Normalized intensity
rf power of $\nu_{A,B}$ [mW]
$\nu_{A,B;(2,0)\leftrightarrow(1,0)}$ = 462.264 MHz (8G)
$\nu_{C;(2,0)\leftrightarrow(2,1)}$ = 113.380 MHz (0.65T)
$S_{A,B}$
S_{A+B+C}
S_{A+B}

Fig. 8

B. Altoon, O. Boyle, P. Colrain, I. ten Have, J.G. Lynch, W. Maitland, W.T. Morton, C. Raine, J.M. Scarr, K. Smith, A.S. Thompson, R.M. Turnbull

Department of Physics and Astronomy, University of Glasgow, Glasgow G12 8QQ,United Kingdom[11]

B. Brandl, O. Braun, R. Geiges, C. Geweniger, P. Hanke, V. Hepp, E.E. Kluge, Y. Maumary, A. Putzer, B. Rensch, A. Stahl, K. Tittel, M. Wunsch

Institut für Hochenergiephysik, Universität Heidelberg, 6900 Heidelberg, Fed. Rep. of Germany[17]

A.T. Belk, R. Beuselinck, D.M. Binnie, W. Cameron, M. Cattaneo, D.J. Colling, P.J. Dornan,[1] S. Dugeay, A.M. Greene, J.F. Hassard, N.M. Lieske, J. Nash, S.J. Patton, D.G. Payne, M.J. Phillips, J.K. Sedgbeer, I.R. Tomalin, A.G. Wright

Department of Physics, Imperial College, London SW7 2BZ, United Kingdom[11]

E. Kneringer, D. Kuhn, G. Rudolph

Institut für Experimentalphysik, Universität Innsbruck, 6020 Innsbruck, Austria[19]

C.K. Bowdery, T.J. Brodbeck, A.J. Finch, F. Foster, G. Hughes, D. Jackson, N.R. Keemer, M. Nuttall, A. Patel, T. Sloan, S.W. Snow, E.P. Whelan

Department of Physics, University of Lancaster, Lancaster LA1 4YB, United Kingdom[11]

K. Kleinknecht, J. Raab, B. Renk, H.-G. Sander, H. Schmidt, F. Steeg, S.M. Walther, B. Wolf

Institut für Physik, Universität Mainz, 6500 Mainz, Fed. Rep. of Germany[17]

J-J. Aubert, C. Benchouk, V. Bernard, A. Bonissent, J. Carr, P. Coyle, J. Drinkard, F. Etienne, S. Papalexiou, P. Payre, Z. Qian, D. Rousseau, P. Schwemling, M. Talby

Centre de Physique des Particules, Faculté des Sciences de Luminy, IN^2P^3-CNRS, 13288 Marseille, France

S. Adlung, C. Bauer, W. Blum,[1] D. Brown, G. Cowan, B. Dehning, H. Dietl, F. Dydak,[24] M. Fernandez-Bosman, M. Frank, A.W. Halley, J. Lauber, G. Lütjens, G. Lutz, W. Männer, R. Richter, H. Rotscheidt, J. Schröder, A.S. Schwarz, R. Settles, H. Seywerd, U. Stierlin, U. Stiegler, R. St. Denis, M. Takashima,[4] J. Thomas,[4] G. Wolf

Max-Planck-Institut für Physik, Werner-Heisenberg-Institut, 8000 München, Fed. Rep. of Germany[17]

V. Bertin, J. Boucrot, O. Callot, X. Chen, A. Cordier, M. Davier, J.-F. Grivaz, Ph. Heusse, P. Janot, D.W. Kim,[20] F. Le Diberder, J. Lefrançois, A.-M. Lutz, M.-H. Schune, J.-J. Veillet, I. Videau, Z. Zhang, F. Zomer

Laboratoire de l'Accélérateur Linéaire, Université de Paris-Sud, IN^2P^3-CNRS, 91405 Orsay Cedex, France

D. Abbaneo, S.R. Amendolia, G. Bagliesi, G. Batignani, L. Bosisio, U. Bottigli, C. Bradaschia, M. Carpinelli, M.A. Ciocci, R. Dell'Orso, I. Ferrante, F. Fidecaro, L. Foà, E. Focardi, F. Forti, A. Giassi, M.A. Giorgi, F. Ligabue, E.B. Mannelli, P.S. Marrocchesi, A. Messineo, F. Palla, G. Rizzo, G. Sanguinetti, J. Steinberger, R. Tenchini, G. Tonelli, G. Triggiani, C. Vannini, A. Venturi, P.G. Verdini, J. Walsh

Dipartimento di Fisica dell'Università, INFN Sezione di Pisa, e Scuola Normale Superiore, 56010 Pisa, Italy

J.M. Carter, M.G. Green, P.V. March, Ll.M. Mir, T. Medcalf, I.S. Quazi, J.A. Strong, L.R. West

Department of Physics, Royal Holloway & Bedford New College, University of London, Surrey TW20 OEX, United Kingdom[11]

D.R. Botterill, R.W. Clifft, T.R. Edgecock, M. Edwards, S.M. Fisher, T.J. Jones, P.R. Norton, D.P. Salmon, J.C. Thompson

Particle Physics Dept., Rutherford Appleton Laboratory, Chilton, Didcot, Oxon OX11 OQX, United Kingdom[11]

B. Bloch-Devaux, P. Colas, H. Duarte, W. Kozanecki, M.C. Lemaire, E. Locci, S. Loucatos, E. Monnier, P. Perez, F. Perrier, J. Rander, J.-F. Renardy, A. Roussarie, J.-P. Schuller, J. Schwindling, D. Si Mohand, B. Vallage

Service de Physique des Particules, DAPNIA, CE-Saclay, 91191 Gif-sur-Yvette Cedex, France[18]

R.P. Johnson, A.M. Litke, G. Taylor, J. Wear

Institute for Particle Physics, University of California at Santa Cruz, Santa Cruz, CA 95064, USA[34]

J.G. Ashman, W. Babbage, C.N. Booth, C. Buttar, R.E. Carney, S. Cartwright, F. Combley, F. Hatfield, P. Reeves, L.F. Thompson[1]

Department of Physics, University of Sheffield, Sheffield S3 7RH, United Kingdom[11]

E. Barberio, A. Böhrer, S. Brandt, C. Grupen, L. Mirabito,[29] F. Rivera, U. Schäfer

Fachbereich Physik, Universität Siegen, 5900 Siegen, Fed. Rep. of Germany[17]

G. Ganis,[33] G. Giannini, B. Gobbo, F. Ragusa[23]

Dipartimento di Fisica, Università di Trieste e INFN Sezione di Trieste, 34127 Trieste, Italy

L. Bellantoni, W. Chen, D. Cinabro,[32] J.S. Conway, D.F. Cowen,[22] Z. Feng, D.P.S. Ferguson, Y.S. Gao, J. Grahl, J.L. Harton, R.C. Jared,[7] B.W. LeClaire, C. Lishka, Y.B. Pan, J.R. Pater, Y. Saadi, V. Sharma, M. Schmitt, Z.H. Shi, A.M. Walsh, F.V. Weber, M.H. Whitney, Sau Lan Wu, X. Wu, G. Zobernig

Department of Physics, University of Wisconsin, Madison, WI 53706, USA[12]

---

†Deceased.

[1]Now at CERN, PPE Division, 1211 Geneva 23, Switzerland.

[2]Permanent address: SLAC, Stanford, CA 94309, USA

[3]Permanent address: University of Washington, Seattle, WA 98195, USA.

[4]Now at SSCL, Dallas, TX, U.S.A.

[5]Also Istituto di Fisica Generale, Università di Torino, Torino, Italy.

[6]Also Istituto di Cosmo-Geofisica del C.N.R., Torino, Italy.

[7]Permanent address: LBL, Berkeley, CA 94720, USA.

[8]Supported by CICYT, Spain.

[9]Supported by the National Science Foundation of China.

[10]Supported by the Danish Natural Science Research Council.

[11]Supported by the UK Science and Engineering Research Council.

[12]Supported by the US Department of Energy, contract DE-AC02-76ER00881.

[13]Supported by the US Department of Energy, contract DE-FG05-87ER40319.

[14]Supported by the NSF, contract PHY-8451274.

[15]Supported by the US Department of Energy, contract DE-FC0S-85ER250000.

[16]Supported by SLOAN fellowship, contract BR 2703.

[17]Supported by the Bundesministerium für Forschung und Technologie, Fed. Rep. of Germany.

[18]Supported by the Direction des Sciences de la Matière, C.E.A.

[19]Supported by Fonds zur Förderung der wissenschaftlichen Forschung, Austria.

[20]Supported by the Korean Science and Engineering Foundation and Ministry of Education.

[21]Supported by the World Laboratory.

[22]Now at California Institute of Technology, Pasadena, CA 91125, USA.

[23]Now at Dipartimento di Fisica, Università di Milano, Milano, Italy.

[24]Also at CERN, PPE Division, 1211 Geneva 23, Switzerland.

[25]Now at DESY, Hamburg, Germany.

[26]Now at University of California at Santa Barbara, Santa Barbara, CA 93106, USA.

[27]Now at TRIUMF, Vancouver, B.C., Canada.

[28]Now at Lufthansa, Hamburg, Germany.

[29]Now at Institut de Physique Nucléaire de Lyon, 69622 Villeurbanne, France.

[30]Also at Università di Napoli, Dipartimento di Scienze Fisiche, Napoli, Italy.

[31]On leave of absence from IHEP, Beijing, The People's Republic of China.

[32]Now at Harvard University, Cambridge, MA 02138, U.S.A.

[33]Supported by the Consorzio per lo Sviluppo dell'Area di Ricerca, Trieste, Italy.

[34]Supported by the US Department of Energy, grant DE-FG03-92ER40689.

[35]Visitor from University of Wisconsin, Madison, WI 53706, USA.

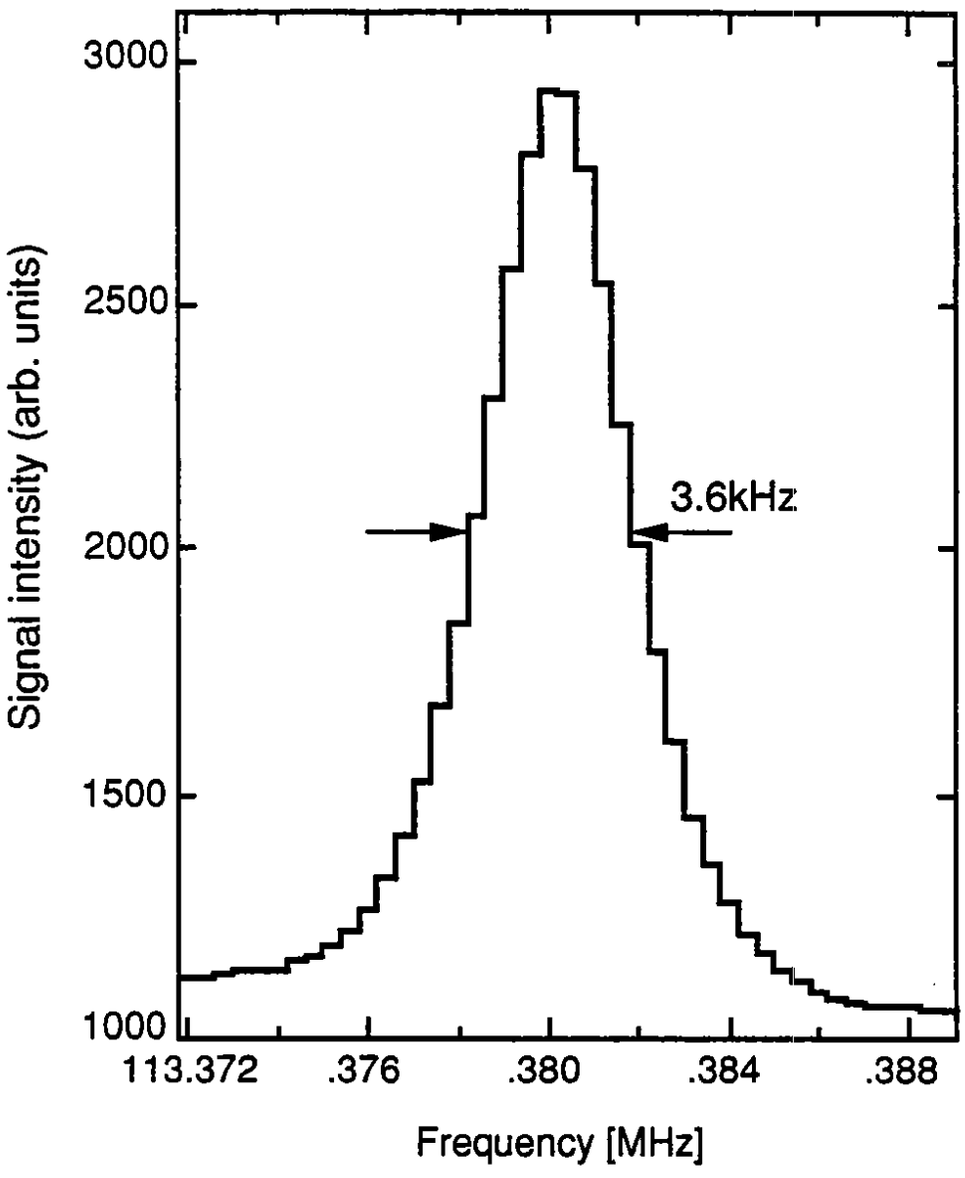
3000
2500
2000
1500
1000
Signal intensity (arb. units)
3.6kHz
113.372
.376
.380
.384
.388
Frequency [MHz]

Fig. 9